Code-modulated interferometric imaging system using phased arrays

Vikas Chauhan, Kevin Greene, and Brian Floyd

Dept. of Electrical and Computer Engineering, North Carolina State University, Raleigh, NC USA 27695

ABSTRACT

Millimeter-wave (mm-wave) imaging provides compelling capabilities for security screening, navigation, and biomedical applications. Traditional scanned or focal-plane mm-wave imagers are bulky and costly. In contrast, phased-array hardware developed for mass-market wireless communications and automotive radar promise to be extremely low cost. In this work, we present techniques which can allow low-cost phased-array receivers to be reconfigured or re-purposed as interferometric imagers, removing the need for custom hardware and thereby reducing cost. Since traditional phased arrays power combine incoming signals prior to digitization, orthogonal code-modulation is applied to each incoming signal using phase shifters within each front-end and two-bit codes. These code-modulated signals can then be combined and processed coherently through a shared hardware path. Once digitized, visibility functions can be recovered through squaring and code-demultiplexing operations. Provided that codes are selected such that the product of two orthogonal codes is a third unique and orthogonal code, it is possible to demultiplex complex visibility functions directly. As such, the proposed system modulates incoming signals but demodulates desired correlations. In this work, we present the operation of the system, a validation of its operation using behavioral models of a traditional phased array, and a benchmarking of the code-modulated interferometer against traditional interferometer and focal-plane arrays.

Keywords: mm-wave, imaging, interferometry, phased array, orthogonal codes, code modulation, Walsh.

1. INTRODUCTION

Millimeter-wave (mm-wave) imagers operating in the range of 30-300 GHz can be used to see through clothes, dust storm, clouds, fog, *etc.* and find applications in surveillance cameras, aircraft navigation, concealed-object detection, and biomedical imaging of wounds or burns. A variety of mm-wave imaging systems have been developed to date [1]. Many of these use optical beam forming with mechanical scanning [2], electronic beam forming and scanning [3] or focal-plane arrays (FPA) [4]. These cameras can be bulky due to the use of an external lens, and expensive due to the reliance on custom compound-semiconductor hardware for scanned solutions or the need for a large number of detecting elements in FPA solutions.

An alternative approach which has the potential to reduce both camera volume and camera cost is to shift to interferometry. Interferometry or synthetic aperture radiometer (SAR) [5, 6] eliminates the need for a lens since angle-of-arrival information is obtained. Furthermore, the number of required elements is reduced, since N elements can be used to obtain ${}^{N}C_{2}$ correlations or visibilities. A drawback of interferometry is the more complicated image processing arising from the need to determine all pairwise complex correlations and compute the Fourier transform. Because of this, the ideal technology for realizing an interferometer would be one having both high-performance mm-wave transistors and dense low-power digital computation [7]. These requirements can now be met in today's advanced silicon technologies, *e.g.*, 130-nm SiGe BiCMOS or 65-nm CMOS, which both feature transistors having f_T and f_{MAX} in excess of 200 GHz.

While it is possible to develop a highly-integrated mm-wave interferometer in silicon, such a customized circuit would require non-negligible development costs. Also, if the total mm-wave camera market volume remains low, the unit cost would remain high. In contrast to this, high-volume mm-wave applications are emerging, including 60-GHz phased arrays for short-range multi-Gb/s wireless links [8] and 77-GHz phased arrays for automotive

Email: vchauha@ncsu.edu, kbgreen2@ncsu.edu, and bafloyd@ncsu.edu

radar systems [9]. These commercial-of-the-shelf (COTS) phased arrays have the potential be used in other multi-antenna applications, allowing for substantial cost reduction. In this work, we explore the possibility of turning a COTS phased array receiver into an interferometric imaging receiver.

The paper is organized as follows. The basics of interferometry are reviewed in section 2 along with the basic hardware requirements of a conventional interferometer. In section 3, we show how a conventional phased array can be reconfigured into an interferometer through the use of code-modulation techniques. We then discuss a demodulation technique which exploits code-set properties to allow for direct demodulation of visibilities. Finally, section 4 summarizes behavioral modeling results and expected system performance.

2. INTERFEROMETRY FUNDAMENTALS

As is well known, interferometry is a technique used by radio astronomers to realize higher resolution telescopes using a sparse array of coherent detectors to sample an aperture [5]. Measurements are made by cross correlating the signals from spatially separated pairs of antennas (a baseline) with overlapping field-of-view (FOV) known as visibility samples. Measurements for different baselines, collectively known as the visibility function, $V(u,v)$, are related to the brightness distribution, T_Ω through a Fourier transform, as follows [10]

$$V(u,v) = \int_0^{2\pi} \int_0^{\pi} T_\Omega(\theta,\phi).\ e^{j2\pi(usin\theta cos\phi + vsin\theta sin\phi)}\ sin\theta\ d\theta\ d\phi\ . \tag{1}$$

Interferometers must therefore evaluate (complex) correlations for each baseline and then compute the inverse Fourier transform to obtain the image. Interferometry does not require a focusing lens, allowing for flat or conformal imagers. Note that image resolution is related to the number of independent baselines, and measurements from redundant baselines can be averaged to reduce noise.

Minimum antenna spacing determines the field of view (FOV), $\theta_{max} \approx \lambda/D_{min}$, whereas maximum angular spacing determines the angular resolution, $\Delta\theta \approx \lambda/D_{max}$ [11]. The ma,ximum antenna spacing (and hence minimum angular resolution) is limited by the coherence requirement [3, 12] as follows

$$D_{max} sin\ \theta_{max} < \frac{c}{B}\ , \tag{2}$$

where c is the velocity of light and B is the bandwidth. More details about interferometry, Nyquist criterion for u-v sampling, correlators and other requirements can be found in [5, 10, 11].

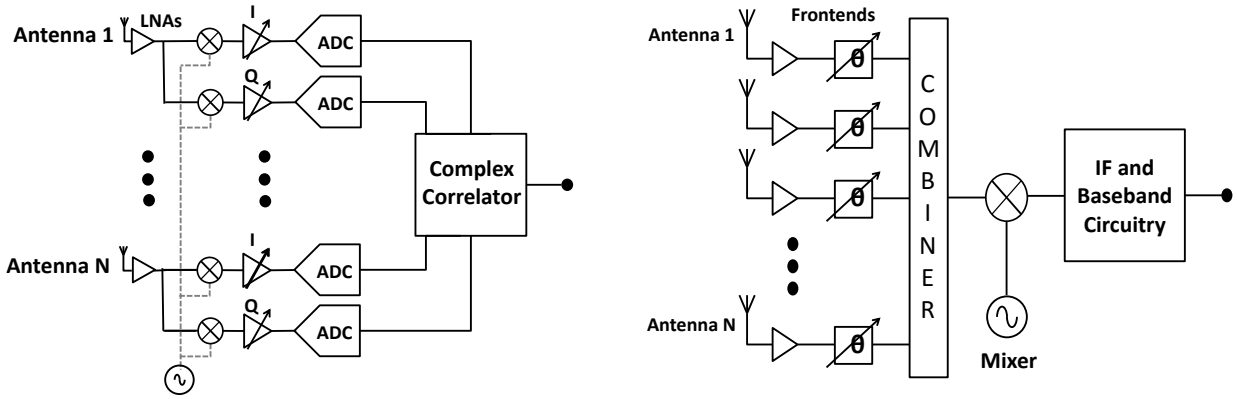

(a) (b)

Figure 1. (a) Block diagram of a conventional interferometric array and (b) Block diagram of a conventional phased array employing RF phase shifting and combining.

Since an interferometer must measure each antenna signal and since the correlations are typically evaluated in the digital domain, an ideal interferometer array would include N receive chains in parallel, as shown in Fig. 1(a). Each chain would generally include a front-end amplifier, a quadrature downconversion mixer, and baseband analog-to-digital converters (ADCs). A bank of digital complex correlators would then be used to evaluate all possible pairwise correlations.

In contrast to this digital-combined array, Fig. 1(b) shows a simplified block diagram of a conventional phased array. Each front-end element contains an RF amplifier and phase-shifter. Individual signals are then added together, downconverted, and processed through to the digital domain. In comparing the phased array to the ideal interferometer array, we observe that the interferometer has individual hardware paths per element whereas the phased array has a shared hardware path beginning at the signal combiner. As a result, any attempt to use a phased array as an interferometer array must allow for the shared hardware path, while retaining necessary individual signal information and/or signal correlations.

3. CODE-MODULATED INTERFEROMETRY WITH PHASED ARRAYS

3.1 Modulation of Antenna Responses

A phased array can be reconfigured into an interferometer array by applying orthogonal coding functions to each incoming signal using the phase shifters present within each front end. Code modulation allows multiple, individual radiometer data streams to be multiplexed onto a single hardware path. As will be shown, we can then recover correlations between signals downstream through correlating the aggregate response with code products.

The speed of the codes relates to the rate of the signal or scene change. In conventional code-modulated communications (*e.g.*, CDMA), the data signals are modulated with a code running at a significantly higher frequency than the modulation or symbol rate. For imaging applications, the signals are being modulated proportional to the scene change; hence, the code rate can be kept low.

The use of code-modulation within receivers has been studied in prior work in the context of either imaging or communications. First for imaging, code modulation has been used within correlating interferometers to eliminate unwanted performance artifacts such as LO feedthrough or spurious signals [5]. Second for communications, code modulations have been applied within a receiver to allow multiple receiver element to share a common hardware path [13]; however, the concepts in [13] were not implemented within an N-element phased array. Our demodulation approach which recovers correlations rather than signals further distinguishes our work over this prior art.

Mathematically, the phase modulation within each front-end can be represented as

$$s_n(t) = A_n cos(\omega_o t + \theta_n - \phi_n) \ , \tag{3}$$

where $s_n(t)$ represents the signal at the output of the n^{th} phase shifter, A_n and θ_n represent the amplitude and phase of the signal, and ϕ_n represents the phase modulation imparted. We can subdivide this expression into in-phase ($s_{i,n}$) and quadrature-phase ($s_{q,n}$) signal components which are then multiplied by in-phase (i_n) and quadrature-phase (q_n) codes, as follows:

$$s_n(t) = \sqrt{2}cos(\phi_n)[A_n \tfrac{\sqrt{2}}{2} cos(\omega_o t + \theta_n)] + \sqrt{2}sin(\phi_n)[A_n \tfrac{\sqrt{2}}{2} sin(\omega_o t + \theta_n)] = i_n s_{i,n} + q_n s_{q,n} \ . \tag{4}$$

Provided that the phase shifter is at least two bits (true for nearly all phased arrays), then the phase shifter can be used to realize phase shifts of $\pm 45°$ and $\pm 135°$. This turns i_n and q_n into simple ± 1 codes (*i.e.*, $\sqrt{2}cos(\pm 45) = 1$ and $\sqrt{2}cos(\pm 135) = -1$). Note that the application of these "two-level" codes allows us to separately modulate both in-phase and quadrature-phase portions of the signal, which will be used later to obtain both real and imaginary visibility functions.

All N signals are then power combined in the phased array, turning the phased-array signal-combining operation into a code-multiplexing operation. The aggregate signal, s_{sum}, is represented as

$$s_{sum} = k_c \sum_n (i_n s_{i,n} + q_n s_{q,n}) \ . \tag{5}$$

Note that this is a time-varying signal, where the time notation has been dropped (*i.e.*, $s_{sum}(t) \rightarrow s_{sum}$). In our summation, we assume that each path has identical gain and amplitude response, represented with k_c, generally obtained after calibration of the array. Additionally, normalized summations are used, where k_c is allowed to be one, where k_c becomes a scalar applied to all visibilities.

3.2 Demodulation of Complex Visibility Functions

Now that all individual antenna signals have been code multiplexed, they can then be coherently processed through a shared hardware path, including digitization in the ADC. In a traditional code-multiplexing system, to obtain the original signal, we would multiply the code-multiplexed signal with the code corresponding to the signal component of interest and then integrate over the code period. In the case of passive imaging, the incoming signals are noise-like with zero mean and therefore would give zero output after demodulation. As a result, in our system, we defer integration until the final cross-correlation step, essentially merging the demultiplexing and correlation processes.

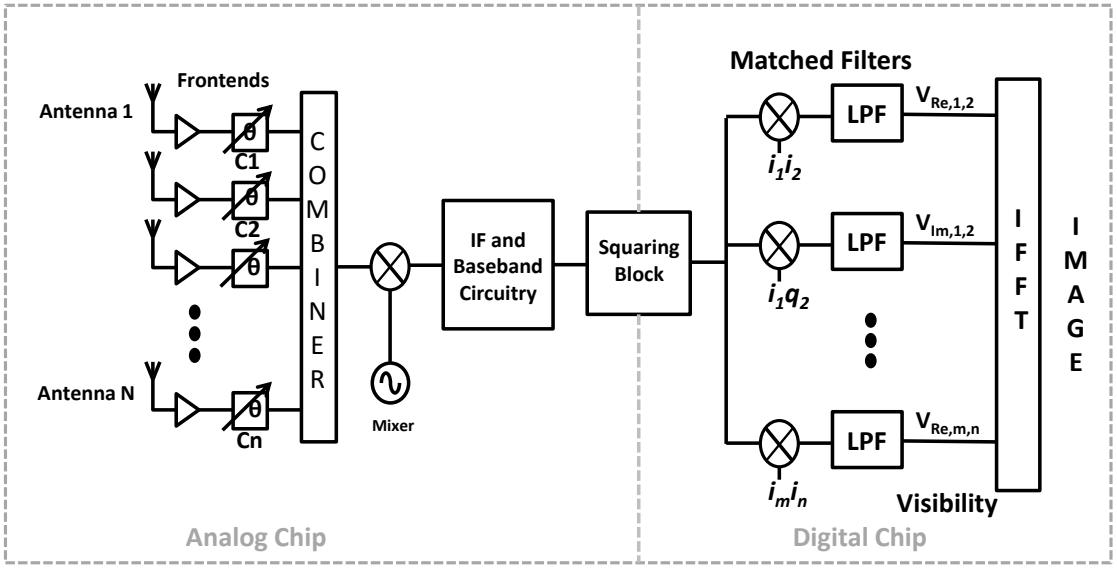

Figure 2. Block diagram of a code-modulated interferometric imaging system employing code-modulation within each phase shifter of a phased array and baseband visibility demodulation using code products.

A block diagram of our proposed system which includes both the code modulation within each front-end and then the visibility demodulation within the digital domain is shown in Fig. 2. For demultiplexing and demodulation, a signal squaring operation is applied to the aggregate s_{sum} signal. Such an operation can be an actual squaring circuit, such as an analog power detector, an RF mixer, a digital squaring operation, or another operation which creates an interference of the code-multiplexed signal with itself. The rationale for such a squaring operation is as follows. In a conventional interferometer, the two signals of interest are correlated or interfered to obtain the visibility products. In Fig. 2 , the aggregate code-multiplexed signal is interfered with itself to obtain all possible visibility products, with the added result that these visibility products are now code modulated [14].

The squared power signal p is represented as

$$p = [s_{sum}]^2 = \sum_n |s_n|^2 + 2\sum_n i_n q_n s_{i,n} s_{q,n} + 2\sum_{n \neq m} (i_n i_m s_{i,n} s_{i,m} + q_n q_m s_{q,n} s_{q,m} + i_n q_m s_{i,n} s_{q,m}) \; . \tag{6}$$

The squared summation or power signal p includes a summation of all of the "self-powers" of the individual signals, a summation of the in-phase to quadrature-phase cross-products of individual signals which are in

general orthogonal to one another and would average to zero, and a summation of all of the code-modulated cross-products between signal pairs.

To demodulate the visibility samples, the power signal is correlated with code products $i_n i_m$ and/or $q_n q_m$ to obtain the real visibility samples. Likewise, the power signal is correlated with code products $i_n q_m$ to obtain the imaginary visibility samples. Since we are correlating the square of the summation with a code product, all code products must be balanced and orthogonal, a property we refer to as "Balanced Orthogonal Code Products" (BOCP). In general, it is possible to have identical code products occur within a set of balanced orthogonal codes. This would result in multiple visibility functions obtained at once or conflicting one with the other. To avoid this, each code product must be balanced and orthogonal.

The resulting visibilities obtained are as follows:

$$v_{Re,n,m} = E(i_n i_m \ . \ p) = 2\overline{s_{i,n} s_{i,m}} \tag{7}$$

$$v_{Im,n,m} = E(i_n q_m \ . \ p) = 2\overline{s_{i,n} s_{q,m}} \tag{8}$$

where the $E(.)$ notation is used to denote the expectation or integration function. In the derivations above, noise has not been included and there will be a component to these visibilities which relates to the average noise values within the system. Additionally, codes have been assumed to be perfectly orthogonal; however, code skew can result in partial correlation between codes leading to residues remaining within the demodulated visibilities.

In summary, our proposed approach to code-modulated interferometry encodes incoming signals using orthogonal codes and decodes desired cross-correlations or visibilities using balanced-orthogonal *code-products*. In particular, the codes must be chosen such that the product of any two codes from the set is a third unique code–the code product. Several different kinds of codes can be used, such as m-sequences, gold codes, or Walsh orthogonal codes. Walsh codes are orthogonal code sets and have been used by the authors for the behavioral results in section 4. For a fixed code length, the product of any two codes from a Walsh set gives a third code from the same set. Walsh codes can be generated using Rademacher codes [15]. For a code of length L, there are $(log_2 L + 1)$ Rademacher codes. For example, for a code of length eight, the four Rademacher codes are

$$\begin{bmatrix} R_0 \\ R_1 \\ R_2 \\ R_3 \end{bmatrix} = \begin{bmatrix} 1 & 1 & 1 & 1 & 1 & 1 & 1 & 1 \\ 1 & 1 & 1 & 1 & -1 & -1 & -1 & -1 \\ 1 & 1 & -1 & -1 & 1 & 1 & -1 & -1 \\ 1 & -1 & 1 & -1 & 1 & -1 & 1 & -1 \end{bmatrix} \tag{9}$$

A complete set of Walsh code generated using these Rademacher codes are $W_1 = R_0$, $W_2 = R_1$, $W_3 = R_1 R_2$, $W_4 = R_2$, $W_5 = R_2 R_3$, $W_6 = R_1 R_2 R_3$, $W_7 = R_1 R_3$ and $W_8 = R_3$.

It is evident that different code pairs can result in same third code (*e.g.*, $W_2 W_3 = W_6 W_7 = W_4$). The BOCP codes used to modulate should be selected such that unique codes are generated by product of any two codes. If $R1, R2$ and $R3$ are used, then only one out of remaining four ($R_1 R_2, R_2 R_3, R_1 R_3$ and $R_1 R_2 R_3$) can be used. For a code length of 1024, 30 such Walsh codes are available. A MATLAB® code was written to identify BOCP code set for any given code length. For a system with N antennas, we need $2N$ codes to be able to obtain complex visibility function from all baselines. With increasing number of antennas, the code length increases significantly and increases the integration time, reducing the frame rate of the imager. Pseudo-random codes could possibly be used in place of Walsh codes to avoid this limitation. Similar challenge is faced in phase switched interferometry and more information can be found in [16].

4. BEHAVIORAL RESULTS AND ANALYSIS

Several behavioral models were created to test the concept using MATLAB® and SIMULINK®. First, conventional interferometry is compared to code-modulated interferometry. An ideal 1-D array of fifteen antennas with wavelength spacing was simulated with receiver noise for each element. Point sources were then swept across elevation angles and the two approaches are compared. The point source consists of a 1-GHz signal with 2-MHz bandwidth to allow for faster computation. The code modulation applied consisted of a chip rate of 1 MHz with

code length 1024. The results for both interferometers were found to be very similar. Fig. 3 shows the plots for one and two point sources at different angles in sky, for conventional and code-modulated interferometry.

The behavioral model was expanded to a two-dimensional scene and imaging array [17]. Fig. 4 shows results for point sources and 2-D "T", "I" and"O" shaped objects. This demonstrates the functionality of the system. Future work includes extending our analysis to quantitatively evaluate variance and sensitivity within our system.

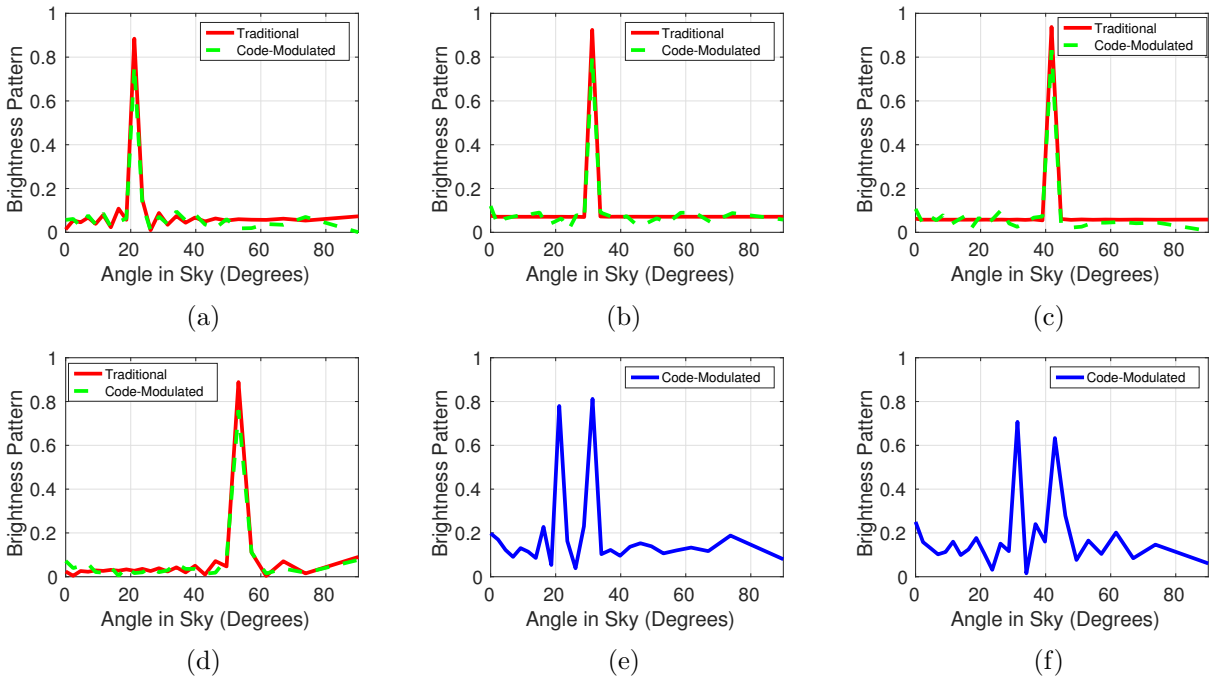

Figure 3. Behavioral modeling results comparing traditional to code-modulated interferometry: (a)-(d) shows the results of a point source at 20°, 30°, 40°, and 50° elevation angles; (e) and (f) show code-modulated interferometry resolving two point sources at elevation angles 20° and 30° in (e), and 30° and 40° in (f).

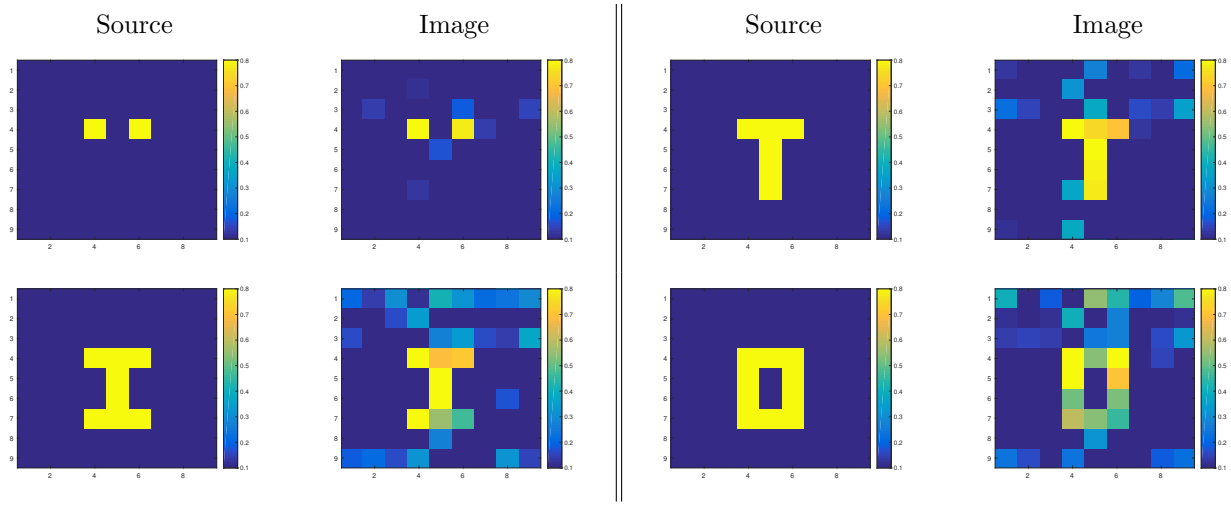

Figure 4. Simulation results for imaging 2-D sources with code-modulated interferometric imaging system.

An important metric for the performance of code modulated interferometry is the sensitivity (ΔT_{min}) defined as the minimum change in temperature of source that can be detected by a radiometer [18]:

$$\Delta T_{min} = \frac{K_e T_{sys}}{\sqrt{\Delta\nu_{HF}\tau_{LF}}} \quad , \tag{10}$$

where K_e is sensitivity constant, T_{sys} is the system noise (T_{sys} = antenna temperature + receiver noise temperature), $\Delta\nu_{HF}$ is the high-frequency bandwidth and τ_{LF} is the integration time. K_e depends upon different factors such as the interferometer configuration or phase switching, correlator/ power detector, *etc.* and can vary between 0.5 and $2\sqrt{2}$ [18] in radio astronomy for single and pairs of antennas. According to [10], unlike in radio astronomy where the source is relatively smaller than the FOV, for the extended sources filling the FOV in imaging, the sensitivity is degraded by the total brightness temperature of the source. Every point in the source contributes to the noise in each visibility point, and therefore to all the pixels in the image. Sensitivity is also affected by the redundancy in baselines, which is worst for a zero-redundancy thinned array ($K_e = \sqrt{N}$) and improving as the array becomes more filled. Comparing with the phase-switched interferometry (K_e =2 for two antennas), the K_e for code-modulated interferometry can be up to N due to summation and subtraction of N different noise sources. This might seem like a huge reduction in sensitivity but the number of pixels obtained could be up to $N(N-1)$ per scan as compared to one pixel per scan in simple interferometer for the same integration time [10].

For an N-element receiver array with 6-dB noise figure ($T_{sys} \approx 1200$ K), RF bandwidths of 1 to 6 GHz, and a frame rate of 30 Hz, $\Delta T_{min} \approx 0.08 \times N$ to $0.21 \times N$. This can be further reduced by using redundant baselines. The code modulation interferometry provides information about all possible baselines and thus redundant information can also be demodulated and used to average out receiver noise. For an array with $D_{min} = \lambda$ the FOV is $\theta_{max} = 1$ rad (approx 60°). For a 60-GHz system with 6-GHz BW, $D_{max} \approx 50$ mm which gives a resolution of 6° which can be reduced to 3° for a ±30° FOV [3]. The resolution can be further improved by dividing the total bandwidth into narrower bandwidths so that the correlation could be extended over larger baselines. Reducing the bandwidth would reduce the sensitivity or increase the integration time for constant sensitivity. This is a trade-off between sensitivity, resolution and frame rate.

Sensitivity and resolution challenges are inherent to using interferometry for radio astronomy and even more stringent for imaging, remote sensing and similar applications. These have been been discussed in detail in [10] with regards to remote sensing. Ample research exists related to interferometry enhancement, including hardware instrumentation, calibration and imaging enhancement algorithms (such as the CLEAN algorithm [5]). These can be applied as well to code-modulated interferometry.

One important challenge for code-modulated interferometry is scalability to larger systems. The Walsh BOCP codes place a hard limit on the number of elements per chip that can be used. A possible solution is to divide the scene into smaller sectors and use multiple chips. Different security or medical applications would require different frame rates and in cases where the cost effectiveness is an important factor, the code-modulated interferometry could prove to be a better option over FPAs and other solutions currently being used.

In summary, with the presented preliminary results from behavioral models, and the analysis for system metrics, code-modulated interferometry appears to be a promising and cost-effective alternative to costly imaging systems present in the market. Future work includes a quantitative analysis of performance and cost. Towards this end, the authors are currently working on building a working prototype using a silicon-based phased array.

ACKNOWLEDGMENTS

This work has been partially funded by a DARPA Young Faculty Award (N66001-11-1-4144) and the 2015 Chancellor's Innovation Fund at NC State University. The authors would like to thank Dr. Zhengxin Tong for his help and preliminary research in the area. The phase array imaging toolbox [17] provided by TxACE (M. Torlak, UT Dallas) was found helpful in implementing the 2D behavioral models.

REFERENCES

[1] Yujiri, L., "Passive millimeter wave imaging," in [*Microwave Symposium Digest, 2006. IEEE MTT-S International*], 98–101 (June 2006).

[2] Yeom, S., Lee, D.-S., Son, J.-Y., Jung, M.-K., Jang, Y., Jung, S.-W., and Lee, S.-J., "Real-time outdoor concealed-object detection with passive millimeter wave imaging," *Opt. Express* **19**, 2530–2536 (Jan 2011).

[3] Lettington, A. H., Dunn, D., Attia, M., and Blankson, I. M., "Passive millimetre-wave imaging architectures," *Journal of Optics A: Pure and Applied Optics* **5**(4), S103 (2003).

[4] Dow, G. S., Lo, D. C. W., Guo, Y., Lin, E. W., Chung, T. T., Biedenbender, M. D., Miromontes, O., Marashi, A., Yujiri, L., Lee, P. S. C., Shoucri, M. M., and Allen, B. R., "Large scale W-band focal plane array for passive radiometric imaging," in [*Microwave Symposium Digest, 1996., IEEE MTT-S International*], **1**, 369–372 (June 1996).

[5] Thompson, A., Moran, J., and Swenson, G., [*Interferometry and Synthesis in Radio Astronomy*], Wiley (2008).

[6] Harvey, A. and Appleby, R., "Prospects for mm-wave aperture synthesis from space-borne and aerial platforms," *Imaging Technology and Telescopes* **4091**, 27–38 (2000).

[7] Pergande, A., "New steps for passive millimeter imaging," *Proc. SPIE* **6548**, 654802–1 – 654802–4 (2007).

[8] Natarajan, A., Reynolds, S. K., Tsai, M. D., Nicolson, S. T., Zhan, J. H. C., Kam, D. G., Liu, D., Huang, Y. L. O., Valdes-Garcia, A., and Floyd, B. A., "A fully-integrated 16-element phased-array receiver in SiGe BiCMOS for 60-GHz communications," *IEEE Journal of Solid-State Circuits* **46**, 1059–1075 (May 2011).

[9] Ku, B. H., Inac, O., Chang, M., and Rebeiz, G. M., "75-85 GHz flip-chip phased array RFIC with simultaneous 8-transmit and 8-receive paths for automotive radar applications," in [*Radio Frequency Integrated Circuits Symposium (RFIC), 2013 IEEE*], 371–374 (June 2013).

[10] Ruf, C. S., Swift, C. T., Tanner, A. B., and Vine, D. M. L., "Interferometric synthetic aperture microwave radiometry for the remote sensing of the Earth," *IEEE Transactions on Geoscience and Remote Sensing* **26**, 597–611 (Sep 1988).

[11] Lim, B. H., *The Design and Development of a Geostationary Synthetic Thinned Aperture Radiometer*, PhD thesis, The University of Michigan (2009).

[12] Skou, N., [*Microwave radiometer systems: Design and analysis*], Norwood, MA, Artech House, page 74 (2006).

[13] Tzeng, F., Jahanian, A., Pi, D., and Heydari, P., "A CMOS code-modulated path-sharing multi-antenna receiver front-end," *IEEE Journal of Solid-State Circuits* **44**, 1321–1335 (May 2009).

[14] B. Floyd, V. Chauhan, K. G., "Code modulated phased array interferometric imaging," disclosure 15106, Provisional Patent Application, USA (06 May 2015).

[15] Henderson, K. W., "Some notes on the Walsh functions," *IEEE Transactions on Electronic Computers* **EC-13**, 50–52 (Feb 1964).

[16] Urry, W. L., "On the use of shifted m-sequences for phase switching or why not complex Walsh functions?," *BIMA* , Technical Memo 76 (09 Aug 1999).

[17] Patole, S. and Torlak, M., "Two dimensional array imaging with beam steered data," *IEEE Transactions on Image Processing* **22**, 5181–5189 (Dec 2013).

[18] Kraus, J., [*Radio Astronomy*], Cygnus-Quasar Books (1986).